

# ULRR

## Molecular sieving and direct visualization of CO<sub>2</sub> in binding pockets of an ultramicroporous lanthanide MOF platform

Item Type	Article
Authors	Han, Lin;Pham, Tony;Zhuo, Mingjing;Forrest, Katherine A.;Suepaul, Shanelle;Space, Brian;Zaworotko, Michael J.;Shi, Wei;Chen, Yao;Cheng, Peng;Zhang, Zhenjie
Citation	ACS Applied Materials and Interfaces;11 (26), pp 23192-23197
Publisher	American Chemical Society
Download date	2026-05-09 23:41:06
Item License	<a href="https://creativecommons.org/licenses/by-nc-sa/1.0/">https://creativecommons.org/licenses/by-nc-sa/1.0/</a>
Link to Item	<a href="https://hdl.handle.net/10344/8239">https://hdl.handle.net/10344/8239</a>

## Molecular Sieving and Direct Visualization of CO<sub>2</sub> in Binding Pockets of An Ultramicroporous Lanthanide MOF Platform

Lin Han, Tony Pham, Mingjing Zhuo, Katherine A. Forrest, Shanelle Suepaul, Brian Space, Michael J. Zaworotko, Wei Shi, Yao Chen, Peng Cheng, and Zhenjie Zhang

*ACS Appl. Mater. Interfaces*, **Just Accepted Manuscript** • DOI: 10.1021/acsami.9b04619 • Publication Date (Web): 11 Jun 2019

Downloaded from <http://pubs.acs.org> on June 17, 2019

### Just Accepted

“Just Accepted” manuscripts have been peer-reviewed and accepted for publication. They are posted online prior to technical editing, formatting for publication and author proofing. The American Chemical Society provides “Just Accepted” as a service to the research community to expedite the dissemination of scientific material as soon as possible after acceptance. “Just Accepted” manuscripts appear in full in PDF format accompanied by an HTML abstract. “Just Accepted” manuscripts have been fully peer reviewed, but should not be considered the official version of record. They are citable by the Digital Object Identifier (DOI®). “Just Accepted” is an optional service offered to authors. Therefore, the “Just Accepted” Web site may not include all articles that will be published in the journal. After a manuscript is technically edited and formatted, it will be removed from the “Just Accepted” Web site and published as an ASAP article. Note that technical editing may introduce minor changes to the manuscript text and/or graphics which could affect content, and all legal disclaimers and ethical guidelines that apply to the journal pertain. ACS cannot be held responsible for errors or consequences arising from the use of information contained in these “Just Accepted” manuscripts.

# Molecular Sieving and Direct Visualization of CO<sub>2</sub> in Binding Pockets of An Ultramicroporous Lanthanide MOF Platform

Lin Han,<sup>†</sup> Tony Pham,<sup>§</sup> Mingjing Zhuo,<sup>¶</sup> Katherine A. Forrest,<sup>§</sup> Shanelle Suepaul,<sup>§</sup> Brian Space,<sup>§</sup> Michael J. Zaworotko,<sup>#</sup> Wei Shi,<sup>†</sup> Yao Chen,<sup>¶</sup> Peng Cheng,<sup>†, ¶</sup> Zhenjie Zhang<sup>†, ‡, ¶, \*</sup>

<sup>†</sup> College of Chemistry, Nankai University, Tianjin, 300071, People's Republic of China.

<sup>‡</sup> Key Laboratory of Advanced Energy Materials Chemistry, Nankai University, Tianjin 300071, People's Republic of China.

<sup>¶</sup> State Key Laboratory of Medicinal Chemical biology, Nankai University, Tianjin 300071, People's Republic of China.

<sup>§</sup> Department of Chemistry, University of South Florida, Tampa Bay Florida 33620-5250, USA.

<sup>#</sup> Department of Chemical Sciences, Bernal Institute, University of Limerick, Limerick V94T9PX, Republic of Ireland.

**ABSTRACT:** Inspired by the structure of carbonic anhydrase, we developed a robust ultramicroporous lanthanide metal-organic framework (MOF) platform (**NKMOF-3-Ln**), which possess porous pocket to selectively bind with CO<sub>2</sub> at ambient condition. Notably, CO<sub>2</sub> molecules can be precisely observed in the single crystal structure of **NKMOF-3-Ln**. Highly ordered CO<sub>2</sub> molecules can strongly interact with framework via electrostatic interaction of nitrates. We found that the CO<sub>2</sub> adsorption capacity and binding energy were gradually enhanced as lanthanide contracting. The strong CO<sub>2</sub> binding affinity endows **NKMOF-3-Ln** excellent CO<sub>2</sub> separation performance, verified by experimental breakthrough results. Moreover, ascribed to the specific binding affinity of CO<sub>2</sub>, **NKMOF-3-Eu** showed fluorescence response to CO<sub>2</sub>.

**KEYWORD:** metal-organic framework, lanthanide, gas separation, CO<sub>2</sub> capture, fluorescence detection

## INTRODUCTION

Host-guest chemistry has been attracting great attention from diverse perspectives including biology, chemistry and materials science.<sup>1</sup> In nature, enzyme molecules can provide a confined environment (pocket) that specifically interact with substrates, which can enhance selective recognition and capture of substrates.<sup>2,3</sup> For example, human carbonic anhydrase II, a classic metalloprotein, can selectively bind with CO<sub>2</sub> molecules via electrostatic interaction or hydrogen binding from amino acids and Zn-bounded hydroxide group (-OH), and thereby facilitating the catalytic process.<sup>4,5</sup> However, precisely determining how substrate molecules interact and bind to their enzyme host is very challenging, but also critical for the understanding of enzymes' structures and functions. Metal-organic frameworks (MOFs) have emerged as a new class of host-guest systems with highly ordered structures,<sup>6,7</sup> tunable pore sizes,<sup>8,9</sup> high surface areas,<sup>10</sup> tailored functionality and facial post-synthetic modification.<sup>11,12</sup> Ascribed to their clear structures, defined pore environment and richness of functional groups (e.g. -NH<sub>2</sub>, -COOH, -OH),<sup>13</sup> MOFs can provide porous pockets to selectively bind with guest molecules, and also facilitate to precisely determine the specific binding sites of guest molecules. Moreover, the above mentioned selective binding capacity towards guest molecules entitled MOFs to serve for a wide variety of applications, including catalysis,<sup>14-17</sup> gas separation,<sup>18-24</sup> gas storage<sup>25,26</sup> and sensing.<sup>27</sup> For instance, the greenhouse effect caused by the rapid accumulation of CO<sub>2</sub> in atmosphere is attracting great attention.<sup>28</sup> Separation of CO<sub>2</sub> using MOF materials has been demonstrated as a promising route for mitigating CO<sub>2</sub> emissions.<sup>29-32</sup> However, precise determination of CO<sub>2</sub> binding sites in MOF structures is still of great challenge, but crucial for the rational design of MOFs to better serve for highly efficient CO<sub>2</sub> separation and capture. Up to now, most CO<sub>2</sub>

binding sites were simulated via high-resolution neutron powder diffraction or computation study.<sup>33-35</sup> However, the precisely crystallographic determination of CO<sub>2</sub> molecules in MOFs via single crystal x-ray diffraction (SCXRD) was still rarely reported.<sup>36,37</sup>

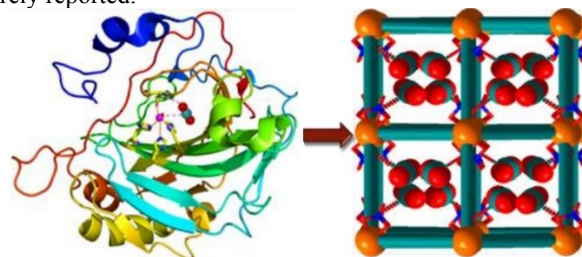


**Figure 1.** Inspired by the host-guest chemistry in enzyme (carbonic anhydrase) to design MOFs with porous pockets to trap CO<sub>2</sub> molecules.

In this study, inspired from the CO<sub>2</sub> binding pocket in the carbonic anhydrase, we introduced strong electrostatic interactions into MOFs and obtained a three-dimensional (3D) ultramicroporous Ln-MOFs (**NKMOF-3-Ln**) platform with specific CO<sub>2</sub> binding affinity (Figure 1). Notably, CO<sub>2</sub> molecules can be clearly visualized in the structure of **NKMOF-3-Ln**, with strong electrostatic interaction from Ln-bounded nitrate group (NO<sub>3</sub><sup>-</sup>). Ascribed to the new type of strong CO<sub>2</sub> binding site and appropriate pore size, **NKMOF-3-Ln** demonstrated sieving effect for CO<sub>2</sub> over N<sub>2</sub> and outstanding separation effect for CO<sub>2</sub>/N<sub>2</sub>. Moreover, we systematically studied the influence of lanthanide contraction effect to the CO<sub>2</sub> sorption/separation. In addition, we also found **NKMOF-3-Eu** demonstrated fluorescence response to CO<sub>2</sub> due to its selective binding affinity. This study paves a new avenue to tune the pore apertures of MOFs in angstrom magnitude via lanthanide contraction effect and provide new

insights into understanding the substrate binding sites in biological systems.

## RESULTS AND DISCUSSION

**Synthesis and characterization of NKMOF-3-Ln platform.**  $(\text{Ln}_2(\text{INO})_4(\text{NO}_3)_2$ , HINO = Isonicotinic acid N-Oxide, Ln = La, Nd, Eu, Dy, Lu), was prepared via solvothermal reactions of  $\text{Ln}(\text{NO}_3)_3$  salts and HINO in DMF/ethanol solvent (Figure S1-S5 and Table S1).<sup>38</sup> Single crystal X-ray diffraction (SCXRD) revealed that there is only one type of Ln(III) atoms which are 9-coordinated with oxygen atoms from the carboxylates and nitrates in **NKMOF-3-Ln**. Two Ln(III) atoms are linked by carboxylates to form a dinuclear secondary building unit (SBU) which can serve as six-connected nodes to link with INO<sup>-</sup> ligands, producing a 3D network of **vmv** topology (Figure S6 and S7). **NKMOF-3-Ln** contains one-dimensional channels along the *a* direction that can accommodate guest molecules (Figure 2a). Interestingly, the Ln-O bond lengths in **NKMOF-3-Ln** series MOFs gradually decreases as lanthanide contracting (Figure S8). As predicted, the lanthanide contraction effect led to the shrinkage of pore size. As summarized in Figure 2b, the distance between the symmetric Ln1A and Ln1B located on the 1D channel wall (Figure S6 and S9) decreased as the atomic numbers increases.<sup>39</sup> The lanthanide contracting effect may affect the adsorption capacity of these materials for CO<sub>2</sub>.

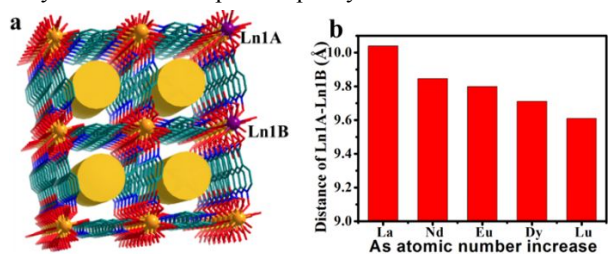


**Figure 2.** (a) Shifted *a*-axis view of the 3D structure of **NKMOF-3-Ln**. (b) Summarization of the distance between Ln1A and Ln1B in **NKMOF-3-Ln**.

**Characterization of NKMOF-3-Ln MOFs.** We found that due to the high connectivity of Ln-SBUs, **NKMOF-3-Ln** displays good stability upon heating or humidity. Thermogravimetric (TG) analysis showed that **NKMOF-3-Nd**, **-Eu**, **-Dy**, and **-Lu** didn't decompose until >250 °C (Figure S10-13). Notably, we observed **NKMOF-3-La** exploded at 350 °C (Figure S14). Powder X-ray diffraction (PXRD) data confirmed the result of TG, and revealed that **NKMOF-3-Ln** can retain their crystallinity upon heating at >250 °C (Figure S15-19). Moreover, we found that the representative **NKMOF-3-Eu** was intact toward 90% humidity for 7 days without losing its crystallinity and porosity (Figure S20 and S21). In order to study the porosity of **NKMOF-3-Ln**, materials were pre-exchanged with MeOH and activated with vacuuming under heating at 160 °C. Surprisingly, the activated **NKMOF-3-Ln** did not adsorb N<sub>2</sub> at 77 K, while adsorbing a relatively large quantity of CO<sub>2</sub> with typical type I isotherms at 195 K (Figure S22-26), thus indicating a molecular sieving effect for CO<sub>2</sub>/N<sub>2</sub>. Based on the CO<sub>2</sub> sorption isotherms, we calculated that the aperture of **NKMOF-3-Ln** is ~4 Å (Figure

S27-31). In order to study if the lanthanide contraction effect influence the gas adsorption/separation performance, we further collected the single-component gas adsorption isotherms for CO<sub>2</sub> and N<sub>2</sub> at 298 K and 273 K. Interestingly, the CO<sub>2</sub> adsorption isotherms displayed very steep curves in the low pressure region and the steepness of the adsorption curves increased with the shrinkage of lanthanides (Figure 3a and S32), which indicated that the binding affinity between the framework and CO<sub>2</sub> gradually increased with the shrinkage of lanthanides. **NKMOF-3-Ln** can adsorb 22.5-24.9 cm<sup>3</sup>/mmol of CO<sub>2</sub> at 1 bar and 298 K, while uptake of N<sub>2</sub> are very low of 2.2-2.6 cm<sup>3</sup>/mmol most likely from particle surface adsorption. These results suggest that **NKMOF-3-Ln** should possess excellent selectivity towards CO<sub>2</sub>/N<sub>2</sub> due to molecular sieving effect. Notably, with increasing the lanthanide atomic numbers, CO<sub>2</sub> uptake exhibits an obvious increasing trend in the entire pressure region. In order to further study the influence of the lanthanide contraction effect to the CO<sub>2</sub> binding affinity, the isosteric heats of adsorption (*Q<sub>st</sub>*) were calculated for **NKMOF-3-Ln** using the virial method (Figure S33-37).<sup>40</sup> It was found that as the atomic number increased, the zero-coverage *Q<sub>st</sub>* values for CO<sub>2</sub> gradually increased from 41 kJ/mol to 58 kJ/mol (Figure 3b). The *Q<sub>st</sub>* value is comparable to that of the benchmark MOFs. These results indicate that the lanthanide contraction effect plays a significant role toward influencing the gas uptakes and binding affinity in these **NKMOF-3-Ln** materials.

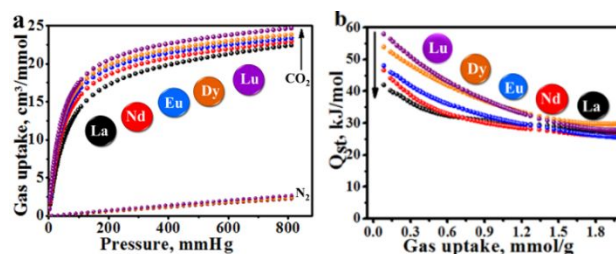


**Figure 3.** (a) Adsorption isotherms of CO<sub>2</sub> and N<sub>2</sub> at 298 K. (b) The *Q<sub>st</sub>* curves of CO<sub>2</sub> for **NKMOF-3-Ln**.

**Single crystal structure of CO<sub>2</sub>@NKMOF-3-Ln.** The steep CO<sub>2</sub> adsorption isotherms in the low pressure region prompted us to study if CO<sub>2</sub> can be captured in the material under ambient conditions. Notably, we found that CO<sub>2</sub> can be trapped in the single crystal structure of **NKMOF-3-Ln** through a very simple approach without sealing or high pressure saturation treatment. Activated **NKMOF-3-Ln** crystals suitable for SCXRD were placed in a CO<sub>2</sub>-filled environment at room temperature with a CO<sub>2</sub> balloon for 8 h. The SCXRD data of **CO<sub>2</sub>@NKMOF-3-Ln** was then collected at 120 K controlled by the liquid nitrogen purge (Table S2). Ascribed to the strong interaction between the structure and CO<sub>2</sub>, we clearly observed the CO<sub>2</sub> molecules without position disorder that facilitate a detailed study of the binding sites between the CO<sub>2</sub> molecules and the framework. Taking **NKMOF-3-Eu** as an example, SCXRD measurements revealed the framework exhibited a unique CO<sub>2</sub> adsorption site. The region between the nitrate and carboxylate from INO<sup>-</sup> is a highly favorable binding site for the CO<sub>2</sub> molecules. The carbon atom in CO<sub>2</sub> molecule possessed strong static electricity interaction with O8 (C13-O8 = 3.07 Å) from the carboxyl group of INO<sup>-</sup> and the O1 (C13-O1 = 3.05 Å) from

the nitrate ion (Figure 4a). We also utilized FT-IR spectroscopy conducted in a N<sub>2</sub> protected glove box to further verify the presence of CO<sub>2</sub> in **NKMOF-3-Eu**. An absorption band at 2335 cm<sup>-1</sup> can be assigned to the stretching vibration of C=O band from the adsorbed CO<sub>2</sub> molecules. Compared with the free linear CO<sub>2</sub> (asym = 2348 cm<sup>-1</sup>), the value is at a lower frequency, which can be assigned to CO<sub>2</sub> interaction with the organic linkers. Due to the strong CO<sub>2</sub>-framework interaction, **NKMOF-3-Eu** can hold CO<sub>2</sub> in its structure for >5 days exposed to air atmosphere without any protection, indicated by the existence of CO<sub>2</sub> signal from FT-IR spectroscopy (Figure 4b).

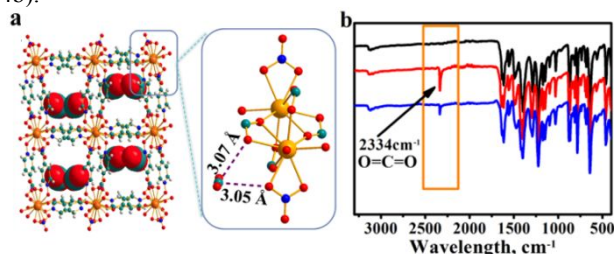


**Figure 4.** (a) CO<sub>2</sub> molecules adsorbed in the single crystal structure of **NKMOF-3-Eu** with strong interaction with NO<sub>3</sub><sup>-</sup> and the INO<sup>-</sup>. C: grey, N: blue, H: white, O: red, Eu: orange. (b) The FT-IR spectra of tested materials, from top to bottom, the activated **NKMOF-3-Eu**; fresh CO<sub>2</sub>@**NKMOF-3-Eu**; CO<sub>2</sub>@**NKMOF-3-Eu** exposed to air for 5 days.

**Molecular simulations.** In order to confirm the SCXRD measurements, molecular simulations of CO<sub>2</sub> adsorption were performed in **NKMOF-3-Eu** to identify the CO<sub>2</sub> binding sites (Figure S38, more details in the Supporting Information). The modeling studies revealed that saturation of CO<sub>2</sub> is achieved at 8 molecules per unit cell (Figure 5b and S39), which is perfectly consistent with the value measured by experimental measurements at 195 K (~8 molecules). The CO<sub>2</sub> molecules prefer to adsorb onto the NO<sub>3</sub><sup>-</sup> counter ions that are coordinated to the Eu<sup>3+</sup> centers in the structure. SCXRD studies of CO<sub>2</sub> adsorbed in **NKMOF-3-Eu** revealed the same adsorption sites. Here, each positively charged C atom of the CO<sub>2</sub> molecule can interact favorably with the electronegative O atom of the NO<sub>3</sub><sup>-</sup> ion. According to the simulated distribution of states within the channels, the simulated C and O positions are in good agreement with the corresponding experimental positions of the CO<sub>2</sub> molecule and the NO<sub>3</sub><sup>-</sup> ions in **NKMOF-3-Eu** (Figure 5a and S40). The strong electrostatic interaction between the CO<sub>2</sub> molecules and NO<sub>3</sub><sup>-</sup> ions within the narrow channels affords a high CO<sub>2</sub> Q<sub>st</sub> in **NKMOF-3-Eu**. The theoretical initial Q<sub>st</sub> values for CO<sub>2</sub> in **NKMOF-3-Eu** calculated to be 47.0 kJ mol<sup>-1</sup>, which is in excellent agreement with the experimental value for **NKMOF-3-Eu**. This supports the experimental finding that the low-loading CO<sub>2</sub> Q<sub>st</sub> in **NKMOF-3-Ln** is close to 50 kJ mol<sup>-1</sup>, indicating strong physisorption interactions between the CO<sub>2</sub> molecules and these MOFs.

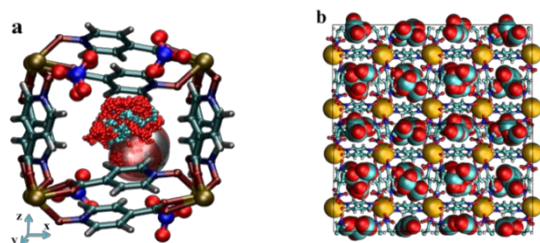


**Figure 5.** (a) Molecular illustration of the simulated distribution of CO<sub>2</sub> molecule positions. (b) Shifted c-axis view of the modeled 4 × 4 × 4 supercell at CO<sub>2</sub> saturation. Atom colors: C = cyan, H = white, N = blue, O = red, Eu = orange.

**IAST selectivity and breakthrough experiments.** The high binding affinity to CO<sub>2</sub> would further benefit materials' CO<sub>2</sub> separation performance. Thus, the gas selectivity calculated via ideal adsorbed solution theory (IAST)<sup>41</sup> based on the gas adsorption isotherms revealed high selectivities (~100-200) for CO<sub>2</sub>/N<sub>2</sub> (15 : 85, v/v) accompanied by an obvious increasing trend as lanthanide atomic number increased in **NKMOF-3-Ln** (Ln = La, Nd, Eu, Dy, Lu) series (Figure S41-46). To further study the separation behavior under a practical application condition, the CO<sub>2</sub>/N<sub>2</sub> separation of **NKMOF-3-Ln** was investigated via column breakthrough experiments using binary CO<sub>2</sub>/N<sub>2</sub> (15:85, v/v) gas mixtures, a typical composition of flue gas mixture from power plants. Notably, all studied **NKMOF-3-Ln** materials exhibit excellent separation performance for CO<sub>2</sub>/N<sub>2</sub> at room temperature. As predicted from the single-component adsorption isotherms, N<sub>2</sub> was firstly eluted through the bed, while CO<sub>2</sub> was adsorbed and retained by **NKMOF-3-Ln**. After >44 min, CO<sub>2</sub> was eluted from the column and quickly reached equilibrium. The retention time of CO<sub>2</sub> (purity > 99.997%) is 44, 51, 55, 59, and 61 min for **NKMOF-3-La**, **-Nd**, **-Eu**, **-Dy**, and **-Lu**, respectively (Figure 6a and S47). This increasing trend in the retention times of **NKMOF-3-Ln** MOFs agrees with the increasing trend of the CO<sub>2</sub> uptake, Q<sub>st</sub> and IAST selectivity in the series, which can be attributed to the lanthanide contraction effect. In order to further investigate the reusability and structural stability of materials during breakthrough experiments, **NKMOF-3-Eu** was evaluated for binary CO<sub>2</sub>/N<sub>2</sub> separation for eight cycles. It can be observed that the retention time remained steady after eight cycles (Figure 6b). Additionally, PXRD data revealed that **NKMOF-3-Eu** retains its crystallinity after recycling experiments (Figure S48) indicative of its excellent regenerability and stability.

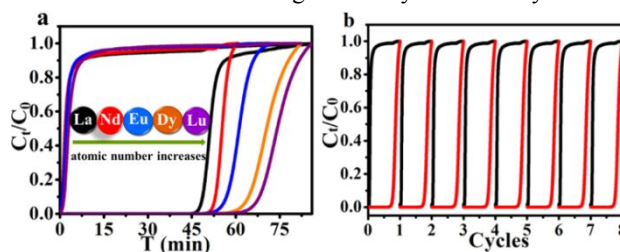


**Figure 6.** (a) Experimental column breakthrough curves of CO<sub>2</sub>/N<sub>2</sub> (15/85) mixtures on **NKMOF-3-Ln** at 298 K and 1.0 bar. (b) Eight cycles of breakthrough experiments of **NKMOF-3-Eu** at 298 K.

**Fluorescence sensing of CO<sub>2</sub>.** Ln-MOFs have drawn intensive attention among the luminescent MOFs due to their unique luminescent properties and great potential as sensors of specific guest molecules.<sup>42-46</sup> Thus, we selected **NKMOF-3-Eu** as a representative to systematically study the fluorescence response properties toward various gases. The activated **NKMOF-3-Eu** was grounded into powder and then suspended

in isopropanol before testing. Isopropanol was chosen as the suspension media due to the following advantages: (i) **NKMOF-3-Eu** was stable in isopropanol verified by PXRD (Figure S49). (ii) Isopropanol cannot enter the pore in **NKMOF-3-Eu** verified by  $^1\text{H}$  NMR due to its large size (4.82 Å) (Figure S50). Excitation of **NKMOF-3-Eu** at 260 nm produced strong emission peak located at 618 nm, which is assigned to the  $^5\text{D}_0 \rightarrow ^7\text{F}_2$  transition of Eu ions. Four weak emission peaks located at 580, 591, 653, and 698 nm were also observed; these peaks are assigned to the following transitions of europium ions:  $^5\text{D}_0 \rightarrow ^7\text{F}_0$ ,  $^5\text{D}_0 \rightarrow ^7\text{F}_1$ ,  $^5\text{D}_0 \rightarrow ^7\text{F}_3$  and  $^5\text{D}_0 \rightarrow ^7\text{F}_4$ , respectively.<sup>47</sup> **NKMOF-3-Eu** shows a fluorescence lifetime of 814  $\mu\text{s}$  with a quantum yield of 24%. Interestingly, when bubbling  $\text{CO}_2$  to the suspension solution of **NKMOF-3-Eu** at room temperature, the intensity of characteristic peaks at 618 nm exhibited a significant change (decreased 74.5% after 1 h). To verify that the decrease of fluorescence intensity was ascribed to the adsorption of  $\text{CO}_2$ , the sample was isolated from isopropanol via centrifugation after bubbling  $\text{CO}_2$  for 0.5 h and 1 h. The FT-IR spectra showed the characteristic stretching vibration of C=O band of  $\text{CO}_2$  (Figure S51). The time-dependent fluorescence changing experiments toward  $\text{CO}_2$  was also performed. The results demonstrate that the fluorescent intensities of characteristic peaks gradually decreased with extending bubbling time. For instance, after bubbling  $\text{CO}_2$  for 6 h, the fluorescent intensities quenched up to 93.3% (Figure 7a). Under excitation of ultraviolet lamp, we can distinguish the fluorescence changes by eyes (Figure S52). Based on the  $\text{CO}_2$  adsorption behavior and SCXRD results, it can be concluded that the guest–host interaction played a significant role in the fluorescence responses of  $\text{CO}_2$ . To further explore if **NKMOF-3-Eu** has high sensing selectivity to  $\text{CO}_2$ , other gases including  $\text{N}_2$ ,  $\text{O}_2$ , He and Ar were tested as well (Figure 7b). Not surprisingly, these gases didn't show significant change for fluorescence intensity of characteristic peaks. These results suggest that the high sensitivity toward  $\text{CO}_2$  can be ascribed to the strong  $\text{CO}_2$  binding affinity. Further study to improve materials' sensing performance toward real applications is ongoing in our lab.

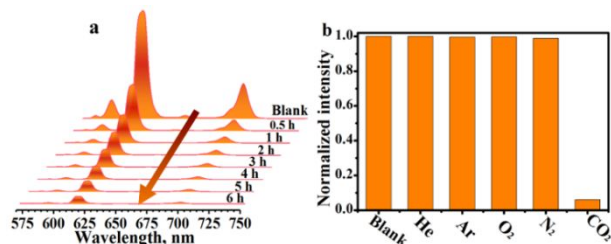


**Figure 7.** (a) Relationship between the fluorescence intensity of activated **NKMOF-3-Eu** in isopropanol and the bubbling time of  $\text{CO}_2$ . (b) Fluorescence intensity changes of **NKMOF-3-Eu** after bubbling  $\text{N}_2$ , He,  $\text{O}_2$ , Ar,  $\text{N}_2$  and  $\text{CO}_2$  for 6 hours.

## CONCLUSION

In summary, we have successfully developed an ultramicroporous 3D lanthanide MOF platform (**NKMOF-3-Ln**), in which the pore aperture can be precisely tuned via the lanthanide contraction effect. The precisely tuned pore diameter significantly enhanced the  $\text{CO}_2$ -framework interaction, as verified by  $\text{CO}_2$  adsorption isotherms and calculation of the  $Q_{\text{st}}$ . Attributed to the strong  $\text{CO}_2$  binding

affinity, we are able to visualize the  $\text{CO}_2$  molecules in the single crystal structure through a facial method under ambient condition and accurately study the binding sites between the  $\text{CO}_2$  molecule and framework. The location of the binding sites was further verified by molecular simulations. **NKMOF-3-Ln** exhibits interesting molecular sieving effect for  $\text{CO}_2/\text{N}_2$  which produced outstanding selectivity for  $\text{CO}_2/\text{N}_2$  (15:85) as verified by IAST calculation and experimental breakthrough results. Moreover, for the first time, we observed that **NKMOF-3-Eu** demonstrated selective fluorescence responses to  $\text{CO}_2$ , due to its specific and strong binding affinity. Our study provides new insight to design MOFs for  $\text{CO}_2$  separation and sensing, and will further broaden the application of MOFs.

## EXPERIMENTAL SECTION

**Synthesis of NKMOF-3-Ln.** In a typical reaction, a mixture of HINO (0.25 mmol),  $\text{Ln}(\text{NO}_3)_3 \cdot 6\text{H}_2\text{O}$  (0.33 mmol), DMF and ethanol were added in a 10 mL glass bottle. Rod like crystals were generated after heating at 80 °C for 48 h. More details are in supporting information.

**Preparation of  $\text{CO}_2$ @NKMOF-3-Ln.** We placed the activated **NKMOF-3-Ln** in a 25 mL glass bottle and sealed with rubber plug, following with vacuuming for 30 minutes. Then, we used a balloon filled with  $\text{CO}_2$  to fill the bottle of **NKMOF-3-Ln** at room temperature. After ~8 h, we chose suitable crystals to collect the single crystal data at 120 K.

**The breakthrough tests:** As for breakthrough test, the samples of **NKMOF-3-Ln** (**NKMOF-3-La**, 1.7343 g; **NKMOF-3-Nd**, 1.7352 g; **NKMOF-3-Eu**, 1.7362 g; **NKMOF-3-Dy**, 1.7289 g; **NKMOF-3-Lu**, 1.7296 g) were exchanged by methanol and activated under He fluxing (20 mL/min) for 500 min at 150 °C in a steel column. Then the breakthrough experiments for  $\text{CO}_2/\text{N}_2$  (15/85, v/v) mixtures were carried out at a flow rate of 2 mL/min (298 K, 1.0 bar). The samples in the column were compressed under the same condition and the column voidages are similar for different samples in order to compare the separation performance. The vertical reactors were placed in a temperature controlled environment, maintained at 298 K. The flow rates of all gases mixtures were regulated by mass flow controllers and the effluent gas stream from the column is monitored by a mass spectrum.

**The fluorescence tests:** The activated **NKMOF-3-Eu** were ground and used for sensing experiments. For each experiment, 5 mg powder of **NKMOF-3-Eu** and 6.0 mL isopropyl alcohol were placed into a small beaker (10 mL), followed by 20 s ultrasonication. The cuvette was then capped and subjected to emission measurements at the wavelength of 260 nanometers as a blank control, after which we bubbled with  $\text{CO}_2$ ,  $\text{N}_2$ , Ar, He or  $\text{O}_2$  to test the change of fluorescence under the same condition.

## ASSOCIATED CONTENT

### Supporting Information

Synthesis, structural figures and supplementary characterization data, cif files, Additional experimental details, FT-IR, gas sorption, breakthrough test, NMR, PXRD, gas sorption, fluorescence test and so on. Supporting information for this article is given via a link at the end of the document.

## AUTHOR INFORMATION

## Corresponding Author

\*zhangzhenjie@nankai.edu.cn

## Author Contributions

The manuscript was written through contributions of all authors. All authors have given approval to the final version of the manuscript.

## Notes

The authors declare no competing financial interests.

## ACKNOWLEDGMENT

The authors acknowledge support of Tianjin Natural Science Foundation of China (18JCZDJC37300) and National Natural Science Foundation of China (21601093). We also acknowledge the National Science Foundation (Award No. DMR-1607989), support from the Major Research Instrumentation Program (Award No. CHE-1531590), ACS Petroleum Research Fund grant (ACS PRF 56673-ND6). Computational resources were made available by a XSEDE Grant (No. TG-DMR090028) and by Research Computing at the University of South Florida. Douglas M. Franz is also acknowledged for calculating the polarizability for  $\text{Eu}^{3+}$ .

## REFERENCES

- (1). Kitagawa, H. Transported into Fuel Cells. *Nat. Chem.* **2009**, *1*, 689-690.
- (2). Ming, T.; Chang, S. *Biomedical Applications of Immobilized Enzymes and Proteins*, Academic Press: Springer Science & Business Media. **2013**, pp 66.
- (3). Cao, L. Q.; Schmid, R. D. *Carrier-bound Immobilized Enzymes: Principles, Application and Design*, Academic Press: John Wiley & Sons. **2010**, pp 38.
- (4). Liang, J. Y.; Lipscomb, W. N. Binding of Substrate  $\text{CO}_2$  to the Active Site of Human Carbonic Anhydrase II: A Molecular Dynamics Study. *Proc. Natl. Acad. Sci. USA.* **1990**, *87*, 3675-3679.
- (5). Merz, K. M.  $\text{CO}_2$  Binding to Human Carbonic Anhydrase II. *J. Am. Chem. Soc.* **1991**, *113*, 406-411.
- (6). Slater, A. G.; Cooper, A. I. Function-led Design of New Porous Materials. *Science* **2015**, *348*, 8075-8084.
- (7). Yin, Z.; Wan, S.; Yang, J.; Kurmoo, M.; Zeng, M. H. Recent Advances in Post-synthetic Modification of Metal-Organic Frameworks: New types and Tandem Reactions. *Coord. Chem. Rev.* **2019**, *378*, 500-512.
- (8). Dolgoplova, E. A.; Brandt, A. J.; Ejegbavwo, O. A.; Duke, A. S.; Maddumapatabandi, T. D.; Galhenage, R. P.; Larson, B. W.; Reid, O. G.; Ammal, S. C.; Heyden, A.; Chandrashekar, M.; Stavila, V.; Chen, D. A.; Shustova, N. B. Electronic Properties of Bimetallic Metal-Organic Frameworks (MOFs): Tailoring the Density of Electronic States through MOF Modularity. *J. Am. Chem. Soc.* **2017**, *139*, 5201-5209.
- (9). Yuan, S.; Zou, L.; Qin, J. S.; Li, J.; Huang, L.; Feng, L.; Wang, X.; Bosch, M.; Alsalme, A.; Cagin, T.; Zhou, H. C. Construction of Hierarchically Porous Metal-Organic Frameworks through Linker Labilization. *Nat. Commun.* **2017**, *8*, 15356.
- (10). Furukawa, H.; Ko, N.; Go, Y.; Aratani, N.; Choi, S.; Choi, E.; Yazaydin, O.; Snurr, R.; O'keeffe, M.; Kim, J.; Yaghi, O. M. Ultrahigh Porosity in Metal-Organic Frameworks. *Science* **2010**, *329*, 424-428.
- (11). MacGillivray, L. R. *Metal-Organic Frameworks: Design and Application*, Academic Press: John Wiley & Sons. **2010**, pp 65.
- (12). García, H.; Navalón, S. *Metal-Organic Frameworks: Applications in Separations and Catalysis*, Academic Press: John Wiley & Sons **2018**, pp 35.
- (13). Zhai, Q. G.; Bu, X.; Mao, C.; Zhao, X.; Daemen, L.; Cheng, Y.; Ramirez-Cuesta, A. J.; Feng, P. An Ultra-tunable Platform for Molecular Engineering of High-Performance Crystalline Porous Materials. *Nat. Commun.* **2016**, *7*, 1-9.
- (14). Wright, A. M.; Wu, Z.; Zhang, G.; Mancuso, J. L.; Comito, R. J.; Day, R. W.; Hendon, C. H.; Miller, J. T.; Dincă, M. A Structural Mimic of Carbonic Anhydrase in a Metal-Organic Framework. *Chem.* **2018**, *4*, 2894-2901.
- (15) Kang, Y. S.; Lu, Y.; Chen, K.; Zhao, Y.; Wang, P.; Sun, W. Y. Metal-organic Frameworks with Catalytic Centers: From Synthesis to Catalytic Application. *Coord. Chem. Rev.* **2019**, *378*, 262-280.
- (16) Zhao, D.; Liu, X. H.; Guo, J. H.; Xu, H. J.; Zhao, Y.; Lu, Y.; Sun, W. Y. Porous Metal-Organic Frameworks with Chelating Multiamine Sites for Selective Adsorption and Chemical Conversion of Carbon Dioxide. *Inorg. Chem.* **2018**, *57* (5), 2695-2704.
- (17) Zhao, D.; Liu, X. H.; Zhu, C.; Kang, Y. S.; Wang, P.; Shi, Z.; Lu, Y.; Sun, W. Y. Efficient and Reusable Metal-Organic Framework Catalysts for Carboxylative Cyclization of Propargylamines with Carbon Dioxide. *ChemCatChem.* **2017**, *9* (24), 4598-4606.
- (18). Belmabkhout, Y.; Bhatt, P. M.; Adil, K.; Pillai, R. S.; Cadiau, A.; Shkurenko, A.; Maurin, G.; Gongping, L.; Koros, W. J.; Eddaoudi, M. Robust Ultramicroporous Metal-Organic Frameworks with Benchmark Affinity for Acetylene. *Nat. Energy* **2018**, *3*, 1059-1066
- (19). Trickett, C. A.; Helal, A.; Al-Maythalyony, B. A.; Yamani, Z. H.; Cordova, K. E.; Yaghi, O. M. The Chemistry of Metal-Organic Frameworks for  $\text{CO}_2$  Capture, Regeneration and Conversion. *Nat. Rev.* **2017**, *2*, 1-16.
- (20) Shan, M.; Liu, X.; Wang, X.; Yarulina, I.; Seoane, B.; Kapteijn, F.; Gascon, J. Facile Manufacture of Porous Organic Framework Membranes for Precombustion  $\text{CO}_2$  Capture. *Sci. Adv.* **2018**, *4* (9), 1-7.
- (21) Luo, F.; Yan, C.; Dang, L.; Krishna, R.; Zhou, W.; Wu, H.; Dong, X.; Han, Y.; Hu, T. L.; O'Keeffe, M.; Wang, L.; Luo, M.; Lin, R.; Chen, B. UTSA-74: A MOF-74 Isomer with Two Accessible Binding Sites per Metal Center for Highly Selective Gas Separation. *J. Am. Chem. Soc.* **2016**, *138* (17), 5678-5684.
- (22) Wang, H.; Dong, X.; Lin, J.; Teat, S. J.; Jensen, S.; Cure, J.; Alexandrov, E. V.; Xia, Q.; Tan, K.; Wang, Q.; Olson, D. H.; Proserpio, D. M.; Chabal, Y. J.; Thonhauser, T.; Sun, J.; Han, Y.; Li, J. Topologically Guided Tuning of Zr-MOF Pore Structures for Highly Selective Separation of  $\text{C}_6$  Alkane Isomers. *Nat. Commun.* **2018**, *9* (1), 1-11.
- (23) Maserati, L.; Meckler, S. M.; Bachman, J. E.; Long, J. R.; Helms, B. A. Diamine-Appended  $\text{Mg}_2(\text{Dobpdc})$  Nanorods as Phase-Change Fillers in Mixed-Matrix Membranes for Efficient  $\text{CO}_2/\text{N}_2$  Separations. *Nano Lett.* **2017**, *17* (11), 6828-6832.
- (24) Shalini, S.; Nandi, S.; Justin, A.; Maity, R.; Vaidhyathanan, R. Potential of Ultramicroporous Metal-Organic Frameworks in  $\text{CO}_2$  Clean-Up. *Chem. Commun.* **2018**, *54* (96), 13472-13490.
- (25). Mason, J. A.; Oktawiec, J.; Taylor, M. K.; Hudson, M. R.; Rodriguez, J.; Bachman, J. E.; Gonzalez, M. I.; Cervellino, A.; Guagliardi, A.; Brown, C. M. Methane Storage in Flexible Metal-Organic Frameworks with Intrinsic Thermal Management. *Nature.* **2015**, *527*, 357-361.
- (26). Zhang, M.; Zhou, W.; Pham, T.; Forrest, K. A.; Liu, W.; He, Y.; Wu, H.; Yildirim, T.; Chen, B.; Space, B. Fine Tuning of MOF-505 Analogues to Reduce Low-Pressure Methane Uptake and Enhance Methane Working Capacity. *Angew. Chem. Int. Ed.* **2017**, *129*, 11584-11588.
- (27). Pan, L.; Liu, G.; Shi, W.; Shang, J.; Leow, W. R.; Liu, Y.; Jiang, Y.; Li, S.; Chen, X.; Li, R. Mechano-Regulated Metal-Organic Framework Nanofilm for Ultrasensitive and Anti-jamming Strain Sensing. *Nat. Commun.* **2018**, *9*, 3813

- (28). Hsiang, S.; Kopp, R.; Jina, A.; Hsiang, S.; Kopp, R.; Jina, A.; Rising, J.; Delgado, M.; Mohan, S.; Rasmussen, D. J. Estimating Economic Damage from Climate Change in the United States Publication Date Estimating Economic Damage from Climate Change in the United States. *Science* **2017**, *356*, 1362–1369.
- (29) Xiang, S.; He, Y.; Zhang, Z.; Wu, H.; Zhou, W.; Krishna, R.; Chen, B. Microporous Metal-Organic Framework with Potential for Carbon Dioxide Capture at Ambient Conditions. *Nat. Commun.* **2012**, *3*, 954–959.
- (30) Nugent, P.; Giannopoulou, E. G.; Burd, S. D.; Elemento, O.; Giannopoulou, E. G.; Forrest, K.; Pham, T.; Ma, S.; Space, B.; Wojtas, L.; Eddaoudi, Mohamed.; Zaworotko, M. J. Porous Materials with Optimal Adsorption Thermodynamics and Kinetics for CO<sub>2</sub> Separation. *Nature* **2013**, *495* (7439), 80–84.
- (31) Jiang, Y.; Tan, P.; Qi, S. C.; Liu, X. Q.; Yan, J. H.; Fan, F.; Sun, L. B. Metal-Organic Frameworks with Target-Specific Active Sites Switched by Photoresponsive Motifs: Efficient Adsorbents for Tailorable CO<sub>2</sub> Capture. *Angew. Chem. Int. Ed.* **2019**, *58*, 1–6.
- (32) Qin, T.; Gong, J.; Ma, J.; Wang, X.; Wang, Y.; Xu, Y.; Shen, X.; Zhu, D. A 3D MOF Showing Unprecedented Solvent-Induced Single-Crystal-to-Single-Crystal Transformation and Excellent CO<sub>2</sub> Adsorption Selectivity at Room Temperature. *Chem. Commun.* **2014**, *50* (100), 15886–15889.
- (33). Xiang, S.; He, Y.; Zhang, Z.; Wu, H.; Zhou, W.; Krishna, R.; Chen, B. Microporous Metal-Organic Framework with Potential for Carbon Dioxide Capture at Ambient Conditions. *Nat. Commun.* **2012**, *3*, 954.
- (34). Yang, S.; Sun, J.; Ramirez-Cuesta, A. J.; Callear, S. K.; David, W. I. F.; Anderson, D. P.; Newby, R.; Blake, A. J.; Parker, J. E.; Tang, C. C.; Schröder, M. Selectivity and Direct Visualization of Carbon Dioxide and Sulfur Dioxide in a Decorated Porous Host. *Nat. Chem.* **2012**, *4*, 887–894.
- (35). Nugent, P.; Belmabkhout, Y.; Burd, S. D.; Cairns, A. J.; Luebke, R.; Forrest, K.; Pham, T.; Ma, S.; Space, B.; Wojtas, L.; Eddaoudi, M.; Zaworotko, M. J. Porous Materials with Optimal Adsorption Thermodynamics and Kinetics for CO<sub>2</sub> Separation. *Nature* **2013**, *495*, 80–84.
- (36). Vaidhyanathan, R.; Iremonger, S. S.; Shimizu, G. K. H.; Boyd, P.; Alavi, G. S.; Woo, T. K. Direct Observation and Quantification. *Science* **2010**, *330*, 650–653.
- (37). Zhang, J. P.; Chen, M. X. Optimized Acetylene/Carbon Dioxide Sorption in a Dynamic Porous Crystal. *J. Am. Chem. Soc.* **2009**, *131*, 5516–5521
- (38). Zhang, X.; Vieru, V.; Feng, X.; Liu, J. L.; Zhang, Z.; Na, B.; Shi, W.; Wang, B. W.; Powell, A. K.; Chibotaru, L. F.; Gao, S.; Cheng, P.; Long, J. R. Influence of Guest Exchange on the Magnetization Dynamics of Dilanthanide Single-Molecule-Magnet Nodes within a Metal-Organic Framework. *Angew. Chem. Int. Ed.* **2015**, *54*, 9861–9865.
- (39). Lee, W. R.; Ryu, D. W.; Lee, J. W.; Yoon, J. H.; Koh, E. K.; Hong, C. S. Microporous Lanthanide-Organic Frameworks with Open Metal Sites: Unexpected Sorption Propensity and Multifunctional Properties. *Inorg. Chem.* **2010**, *49*, 4723–4725.
- (40). Czepirski, L.; Jagietto, J. Virial-type Thermal Equation of Gas-Solid Adsorption Leszek. *Chem. Eng. Sci.* **1989**, *44*, 797-801
- (41). Myers, A. L.; Prausnitz, J. M. Thermodynamics of Solid Carbon Dioxide Solubility in Liquid Solvents at Low Temperatures. *Ind. Eng. Chem. Fundam.* **1965**, *11*, 121–127.
- (42). Xu, X. Y.; Yan, B. Eu(III)-Functionalized ZnO@MOF Heterostructures: Integration of Pre-concentration and Efficient Charge Transfer for the Fabrication of A Ppb-Level Sensing Platform for Volatile Aldehyde Gases in Vehicles. *J. Mater. Chem. A.* **2017**, *5*, 2215–2223.
- (43). Yan, Z. H.; Du, M. H.; Liu, J.; Jin, S.; Wang, C.; Zhuang, G. L.; Kong, X. J.; Long, L. S.; Zheng, L. S. Photo-Generated Dinuclear {Eu(II)}<sub>2</sub> Active Sites for Selective CO<sub>2</sub> Reduction in A Photosensitizing Metal-Organic Framework. *Nat. Commun.* **2018**, *9*, 3353.
- (44). Yang, D.; Tian, Y.; Xu, W.; Cao, X.; Zheng, S.; Ju, Q.; Huang, W.; Fang, Z. A Series of Lanthanide-Based Metal–Organic Frameworks: Synthesis, Structures, and Multicolor Tuning of Single Component. *Inorg. Chem.* **2017**, *56*, 2345–2353.
- (45). Ji, G.; Liu, J.; Gao, X.; Sun, W.; Wang, J.; Zhao, S.; Liu, Z. A Luminescent Lanthanide MOF for Selectively and Ultra-high Sensitive Detecting Pb<sup>2+</sup> Ions in Aqueous Solution. *J. Mater. Chem. A.* **2017**, *5*, 10200-10205.
- (46) Jamali, A.; Tehrani, A. A.; Shemirani, F.; Morsali, A. Lanthanide Metal–Organic Frameworks as Selective Microporous Materials for Adsorption of Heavy Metal Ions. *Dalton Trans.*, **2016**, *45*, 9193-9200.
- (47). Gao, Y.; Jing, P.; Yan, N.; Hilbers, M.; Zhang, H.; Rothenberg, G.; Tanase, S. Dual-mode Humidity Detection Using a Lanthanide-Based Metal-Organic Framework: Towards Multifunctional Humidity Sensors. *Chem. Commun.* **2017**, *53*, 4465–4468.

## TOC

